

## RIDER MOTION IDENTIFICATION DURING NORMAL BICYCLING BY MEANS OF PRINCIPAL COMPONENT ANALYSIS

Jason K. Moore, J. D. G. Kooijman and A. L. Schwab

Laboratory for Engineering Mechanics  
Delft University of Technology, Mekelweg 2, 2628CD Delft, The Netherlands  
e-mails: jkmoor@ucdavis.edu, jodikooijman@gmail.com, a.l.schwab@tudelft.nl  
web page: <http://bicycle.tudelft.nl>

**Keywords:** bicycle, principal component analysis, motion capture, human control

**Abstract.** *Recent observations of a bicyclist riding through town and on a treadmill show that the rider uses the upper body very little when performing normal maneuvers and that the bicyclist may in fact primarily use steering input for control. They also revealed that other motions such as lateral movement of the knees were used in low speed stabilization. In order to validate the hypothesis that there is little upper body motion during casual cycling, an in-depth motion capture analysis was performed on the bicycle and rider system.*

*We used motion capture technology to record the motion of three similar young adult male riders riding two different city bicycles on a treadmill. Each rider rode each bicycle while performing stability trials at speeds ranging from 2 km/h to 30 km/h: stabilizing while pedaling normally, stabilizing without pedaling, line tracking while pedaling, and stabilizing with no-hands. These tasks were chosen with the intent of examining differences in the kinematics at various speeds, the effects of pedaling on the system, upper body control motions and the differences in tracking and stabilization.*

*Principal component analysis was used to transform the data into a manageable set organized by the variance associated with the principal components. In this paper, these principal components were used to characterize various distinct kinematic motions that occur during stabilization with and without pedaling. These motions were grouped on the basis of correlation and conclusions were drawn about which motions are candidates for stabilization related control actions.*

## 1 INTRODUCTION

Much progress has been made in understanding the rigid body dynamics of an uncontrolled bicycle [4] and various control schemes have been explored for tracking purposes [7, 8, 9], but little is understood about how a bicyclist actually stabilizes a bicycle during normal riding. A bicycle and rider system is unique among vehicles in the fact that the rider is from 80 to 90 percent of the total mass of the system, the system is laterally unstable and that the rider is flexibly coupled to the bicycle in such a way that many body motions can be used as control inputs. Previous research into realistic bicycle control has focused on both steering and rider lean as control inputs, but there has been no experimental verification of which motions a rider actually uses for control. Recent observations of a bicyclist riding through town and on a treadmill [2] show that the rider moves the upper body very little when performing normal maneuvers and that the bicyclist may in fact primarily use steering input for control. This corresponds well with the fact that control by leaning requires high gains compared to the gains required for steering when employing an optimal control strategy on a model such as LQR [7, 8, 9]. The observations also revealed that the rider may use other control inputs such as drastic knee movements at low speeds. These conclusions were drawn by visually reviewing video data, so a more rigorous objective method of characterizing the dominant movements of the bicyclist while stabilizing a bicycle is needed. In order to validate the hypothesis that there is little upper body motion during normal cycling, motion capture techniques were used on the bicycle and rider system with the intent to use principal component analysis to identify the major motion patterns.

Principal component analysis has successfully been used with data collected from motion capture techniques to identify the dominant modes of motion of a person walking on treadmill [10] and to characterize different types of walking. We use similar methods for steady, normal bicycle riding on a treadmill. Cyclic motions, such as pedaling, are easily identified and separated from the other less cyclic control actions. Identifying the patterns of movement gives insight into which body movements are primarily used and are candidates for control inputs. This will be valuable for design of a realistic biomechanical based control system of a bicycle rider, among other things.

## 2 EXPERIMENTS

To test our hypotheses, three riders performed a set of stability tasks in a controlled environment while the motion of the bicycle and rider were collected with a motion capture system. The tasks were performed on a  $3 \times 5$  meter treadmill Fig. (1) capable of belt speeds up to 35 km/h. The treadmill was chosen because the envelope of space was suitable for the motion capture system and it eliminated any disturbances such as wind, rough ground, and obstacles. We chose three male riders of similar age [27 years ( $\sigma = 4$ )] and build [height= 1.81 m ( $\sigma = 0.04$ ) and mass= 73 kg ( $\sigma = 1$ )]. We also used two different Dutch bicycles: a 2008 Batavus Browser with a 3 speed hub and a 2008 Batavus Stratos Deluxe with a 7 speed hub. The Browser is described by the manufacturer as “stable” and the Stratos Deluxe as “nervous.”

We made use of the Optotrack Certus Motion Capture System [6] to record the motion of the bicycle and rider during the stability tasks. The system is based on active infrared emitting markers that are placed on the moving bodies and connected to a central control unit. Each marker emits an infrared signal at a different frequency and the infrared pulses are captured by camera modules each containing three cameras. The accuracy of the three dimensional measurements is  $\pm 0.15$  mm. Wiring harnesses were built for both the rider and the bicycles to facilitate easy bicycle and rider exchange Fig. (2).



Figure 1: The  $3 \times 5$  m treadmill at the Vrije Universiteit Amsterdam.

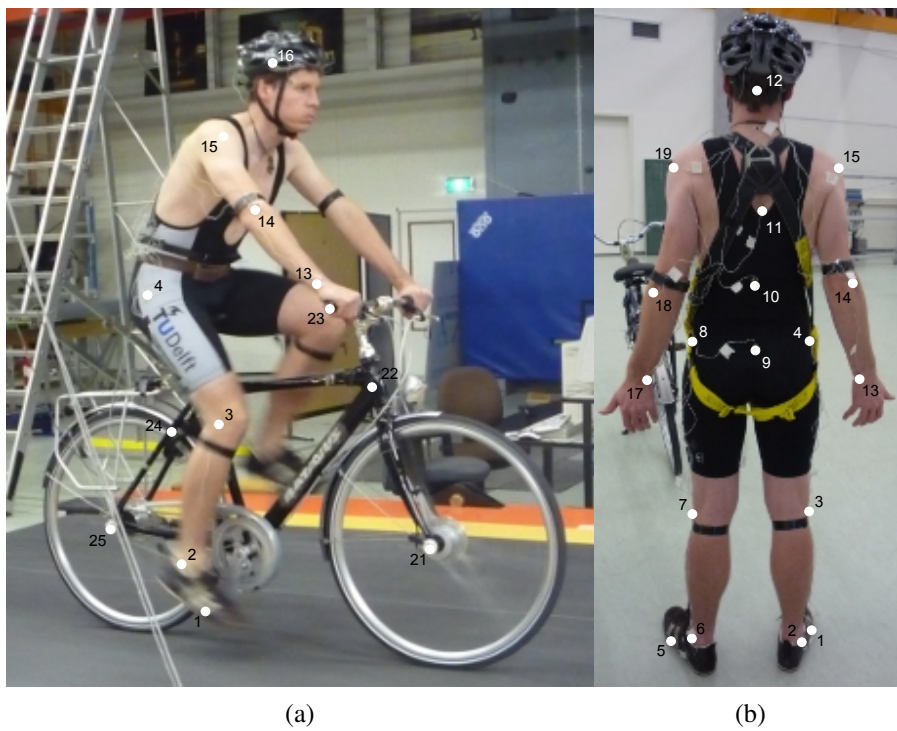


Figure 2: (a) Rider 1 and the Batavus Stratos Deluxe with marker positions. (b) Body marker positions visible from the rear.

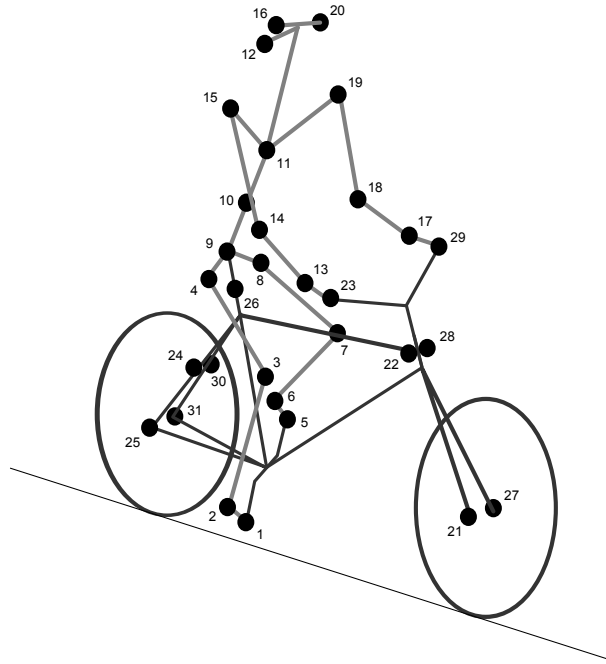


Figure 3: Schematic of the marker positions. The bicycle and rider are colored light gray and dark gray, respectively.

The marker coordinates were measured with respect to an inertial frame,  $M$ , where the plane normal to  $\hat{m}_3$  is coplanar with the treadmill surface and  $\hat{m}_3$  is directed upward. We collected the three dimensional locations of 31 markers, 11 of which were located on the bicycle and 20 that mapped the rider Fig. (3).

The markers were placed on the bicycle so that we could easily extract the rigid body motion (i.e. body orientations and locations) of the bicycle frame and fork. Four markers were attached to the fork and seven markers were attached to the rear frame. A marker was attached on the right and left sides of the center of each wheel, the seat stays, the ends of the handlebars, and the head tube. A single marker was also attached to the back of the seat post.

We recorded the location of 20 points on the rider: left and right sides of the helmet, back of the helmet, shoulders, elbows, wrists, between the shoulder blades on the spine, the midpoint between the shoulder blades and the coccyx, the coccyx, hips, knees, ankles and feet. The body markers were not placed such that a complete rigid body model could easily be fit to the data. This was done to save setup and processing time because we only wanted a stick figure representation of the rider that allowed us to visually observe the dominant motions of the rider.

The stability tasks were designed such that the rider rode at a constant speed within the range of 2 to 30 km/h. The bicyclists were told to maintain an upright straight ahead course on the treadmill and to look into the distance, with exception of the line tracking task. The bicyclists were instructed to bicycle comfortably at the designated speed and the data recording was started at random. In all cases the subject rode at the set speed until comfortable, then data was taken for 60 seconds at a 100 hertz sampling rate. Each test was performed on each bicycle with each rider. The following list gives the various tests and their descriptions:

**Normal pedaling** The subject was instructed to simply stabilize the bicycle while pedaling and keep the heading in approximately the forward direction. The speed started at 5 km/h and increased in 5 km/h increments up to 30 km/h. The speeds were then decreased in the same fashion to 5 km/h. From then on the speed was decreased in 1 km/h increments until

the subject was not able stabilize the bicycle any longer. Therefore, there were two sets of data for each speed and each bicycle except speeds below 5 km/h. Several additional runs were also performed with the rider pedaling using a different gear and thus a different cadence.

**Without pedaling** This was the same as the normal pedaling task except that a string was attached to the head tube of the bicycle such that the bicycle was fixed longitudinally relative to the treadmill and no pedaling was required. The rider kept the feet in the same position throughout the task.

**No-hands** The rider stabilized the bicycle without using steering for control. They were instructed to keep their hands on their hips while bicycling. The rider started at 30 km/h and decreased in 5 km/h increments through 20 km/h and thereafter the speeds were decreased in 1 or 2 km/h increments until the rider was not able to comfortably stabilize the bicycle.

**Line tracking** This was the same as normal pedaling except that the rider was instructed to track a line on the treadmill surface with the front wheel. A smaller subset of speeds was performed.

These tasks were designed with the intent to answer several questions:

1. What upper body motions are used while bicycling?
2. How does the motion of the system change with respect to change in forward speed?
3. How much does pedaling influence the control actions?
4. Can the open loop rigid body dynamics be detected in the controlled state?
5. What does the rider do differently to control the bicycle when riding no-hands?
6. Do different bicyclists perform similar motions while performing the same task?
7. Is there a difference in motion when stabilizing and trying to track a line?

Since there is no room to address all of these questions in this paper, we focus on a single rider on the Browser bicycle and two of the tasks: normal pedaling and without pedaling. We were able to draw some conclusions on questions 1 through 4 with this smaller data set.

### 3 OPEN LOOP RIGID BODY DYNAMICS

One question we have is whether or not the eigenfrequencies of the weave motion for the uncontrolled system can be detected in the results from the stabilization tasks. In order to predict the uncontrolled (open loop) eigenvalues of the rigid rider system, the basic geometry, mass, center of gravity locations, and moments of inertia of the bicycle were measured as in [3]. Also, the riders were measured and weighed such that the body segment geometry, mass, center of gravity locations, and moments of inertia could be estimated using the method described in [5]. This data was used to calculate eigenvalues and eigenvectors of the uncontrolled open loop system Fig. (4).

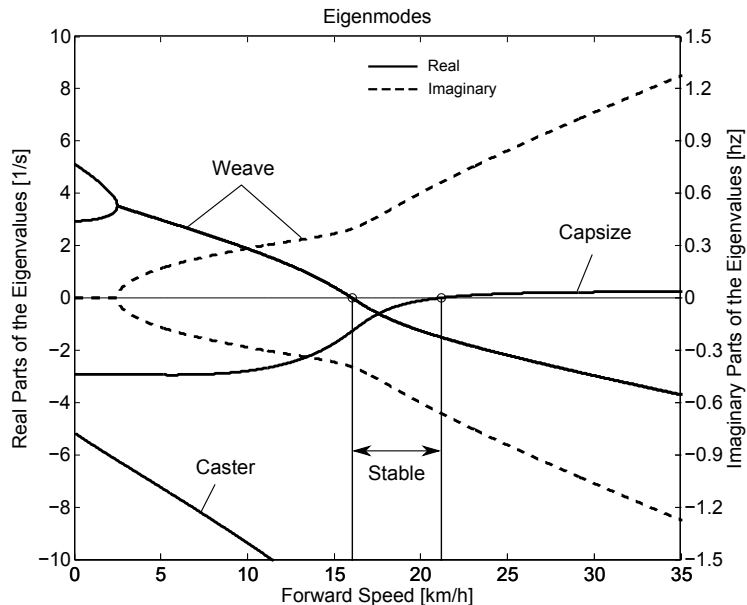


Figure 4: Eigenvalues of the Browser bicycle with the third rider as a function of speed. Note that the initially unstable weave motion becomes stable above 16 km/h, the weave speed.

## 4 DATA PROCESSING

### 4.1 Missing markers

The Optotrack Certus Motion Capture System [6] is based on the cameras' ability to detect the infrared light from the sensors so there are occasional gaps in the coordinate data due to the markers going out of view. We attempted to minimize this by careful marker and camera placement but were not able to totally eliminate the error. Any missing markers on the bicycle were reconstructed using the fact that the bicycle is a rigid body. We had more than three markers on both the frame and fork, so if one marker location was not detected we used the relative location of the remaining markers to reconstruct the missing marker. The gaps in the data of the markers on the human were repaired by fitting a cubic spline through the data. The spline estimated the marker coordinates during the gaps. We only used the splined data if the gaps were less than 10 time steps, or 0.1 sec, otherwise the trials were discarded.

### 4.2 Relative motion

We were interested in the analysis of three different marker combinations: the bicycle, the rider and the bicycle/rider. The motion of the bicycle and the bicycle/rider were calculated with reference to the  $N$  inertial frame and the motion of the rider was calculated with respect to the rear frame of the bicycle  $B$  Fig. (5). These three marker combinations allowed us to differentiate more easily between rider specific and bicycle specific motions. Furthermore, six of the variables that describe the configuration of the bicycle in time were calculated to give insight into the rigid body dynamics. Details of these calculations are shown in Appendix A.

### 4.3 Principal Component Analysis

We used Principal Component Analysis [1] to extract and characterize the dominant motions of the system. Calculating the principal components effectively transforms the space of the

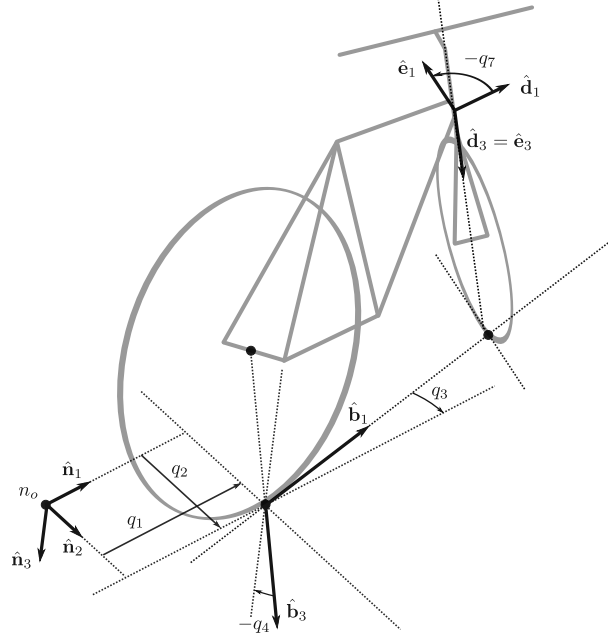


Figure 5: Diagram of the bicycle's inertial frame  $\mathbf{N}$ , rear frame  $\mathbf{B}$ , front frame  $\mathbf{E}$  and configuration variables.

data to a space that maximizes the variance of the data. The typical advantage of PCA is that the dimension of the system can be reduced and still retain enough information to adequately describe the system. We are primarily interested in the way that PCA is able to extract linear components and rank them in order of variance from the mean position. If we assume that the components with the largest kinematic variance are motions that are the dominant motions used for control and propulsion (which in general is not necessarily true for dynamical systems) the comparison of these components for different riding conditions can give insight into what motions may be important for developing a biomechanical control model of the bicyclist.

The repaired data from the motion capture measurements contained the  $x$ ,  $y$ , and  $z$  coordinates of each marker 1 through  $l$  at each time step  $j = 1, 2, \dots, n$ . Each marker has three coordinates so there are a total of  $m = 3l$  coordinates  $i = 1, 2, \dots, m$ . The coordinates at each time step can be collected in vector  $\mathbf{p}_j$ .

$$\mathbf{p}_j^T = [x_{1j} \quad \dots \quad x_{lj} \quad y_{1j} \quad \dots \quad y_{lj} \quad z_{1j} \quad \dots \quad z_{lj}] = [p_{1j} \quad p_{2j} \quad \dots \quad p_{mj}]$$

We can organize these coordinate vectors into a matrix,  $\mathbf{P}$ , where the rows,  $i$ , map a single coordinate of a marker through  $n$  time steps.

$$\mathbf{P} = \begin{bmatrix} | & | & & | & & | \\ \mathbf{p}_1 & \mathbf{p}_2 & \dots & \mathbf{p}_j & \dots & \mathbf{p}_n \\ | & | & & | & & | \end{bmatrix}$$

The principal components were calculated for the three marker combinations as described earlier where  $n = 60 \cdot 100 = 6000$  time steps. The number of rows of  $\mathbf{P}$  were ( $m = 3 \cdot 31 = 93$ ), ( $m = 3 \cdot 11 = 33$ ) and ( $m = 3 \cdot 21 = 63$ ) for the bicycle/rider, the bicycle alone and the rider alone, respectively.

One method of determining the principal components is to calculate the eigenvectors of the covariance matrix of the mean-subtracted data. We begin by calculating the mean Eq. (1) of the

rows of  $\mathbf{P}$  and subtracting it from each column of  $\mathbf{P}$  to form the mean-subtracted data matrix  $\mathbf{B}$  Eq. (2).

$$\mathbf{u} = \frac{1}{n} \sum_{j=1}^n \mathbf{P}_j \quad (1)$$

A vector of ones

$$\mathbf{h}^T = [h_1 \quad h_2 \quad \dots \quad h_j \quad \dots \quad h_n] \text{ where } h_j = 1 \text{ for all } j$$

allows us to subtract  $\mathbf{u}$  from each column of  $\mathbf{P}$ ,

$$\mathbf{B} = \mathbf{P} - \mathbf{u}\mathbf{h}^T \quad (2)$$

The covariance matrix  $\mathbf{C}$  of  $\mathbf{B}$  can then be calculated with Eq. (3).

$$\mathbf{C} = \frac{1}{n-1} \mathbf{B}\mathbf{B}^T \quad (3)$$

Calculating the eigenvectors  $\mathbf{v}_i$  and eigenvalues  $\lambda_i$  of the covariance matrix effectively transforms the space to one where the variances are maximized and the covariances are zero. The eigenvectors are the principal components of the data set and the corresponding eigenvalues represent the variance of each principal component. The eigenvectors are ordered by decreasing eigenvalue where  $\mathbf{v}_1$  is the eigenvector corresponding to the largest eigenvalue. The eigenvalues and eigenvectors are calculated by finding the independent solutions to Eq. (4).

$$\mathbf{C}\mathbf{v}_i = \lambda_i \mathbf{v}_i \quad (4)$$

Each time step can now be represented as a linear combination of the principal components.

$$\mathbf{p}_j = \mathbf{u} + a_{1j}\mathbf{v}_1 + a_{2j}\mathbf{v}_2 + \dots + a_{mj}\mathbf{v}_m \quad (5)$$

The coefficients  $a_{ij}$  can be solved for each time step  $j$  by reformulating Eq. (5) and solving the system of linear equations.

$$\mathbf{P} - \mathbf{u}\mathbf{h}^T = \begin{bmatrix} | & | & \dots & | \\ \mathbf{v}_1 & \mathbf{v}_2 & \dots & \mathbf{v}_m \\ | & | & \dots & | \end{bmatrix} \begin{bmatrix} a_{11} & \dots & a_{1n} \\ \vdots & \ddots & \vdots \\ a_{m1} & \dots & a_{mn} \end{bmatrix} = \mathbf{V}\mathbf{A} \quad (6)$$

and

$$\mathbf{A} = \mathbf{V}^{-1}(\mathbf{P} - \mathbf{u}\mathbf{h}^T). \quad (7)$$

With the principal components  $\mathbf{v}_i$  being constant, the behavior in time is described by the coefficients  $a_{ij}$  where the discretization in time is indexed by  $j$ . The order of the system can be reduced by eliminating principal components that have little variance. We arbitrarily decided to examine the first  $k = 10$  principal components knowing that the first five would be based around the larger motions such as pedaling and that the remaining five may reveal some of the motions associated with control. The variance of each component,  $\text{var}(\mathbf{a}_i) = \lambda_i$ , is summed to determine the cumulative percentage of variance of the principal components,  $g_k$ .

$$g_k = 100 \frac{\sum_{i=1}^k \lambda_i}{\sum_{i=1}^m \lambda_i} \text{ where } 1 \leq k \leq m \quad (8)$$

Highly correlated data will show that even when  $k \ll m$ ,  $g_k$  is close to 100%. Using 10 components  $g_{10}$  covers 100% ( $\sigma = 2 \cdot 10^{-14}\%$ ) of the variation in the data for the bicycle, rider and bicycle/rider. The matrix  $\mathbf{A}$  can then be reduced to a  $k \times n$  matrix and eigenvectors greater than  $\mathbf{v}_k$  can be eliminated.

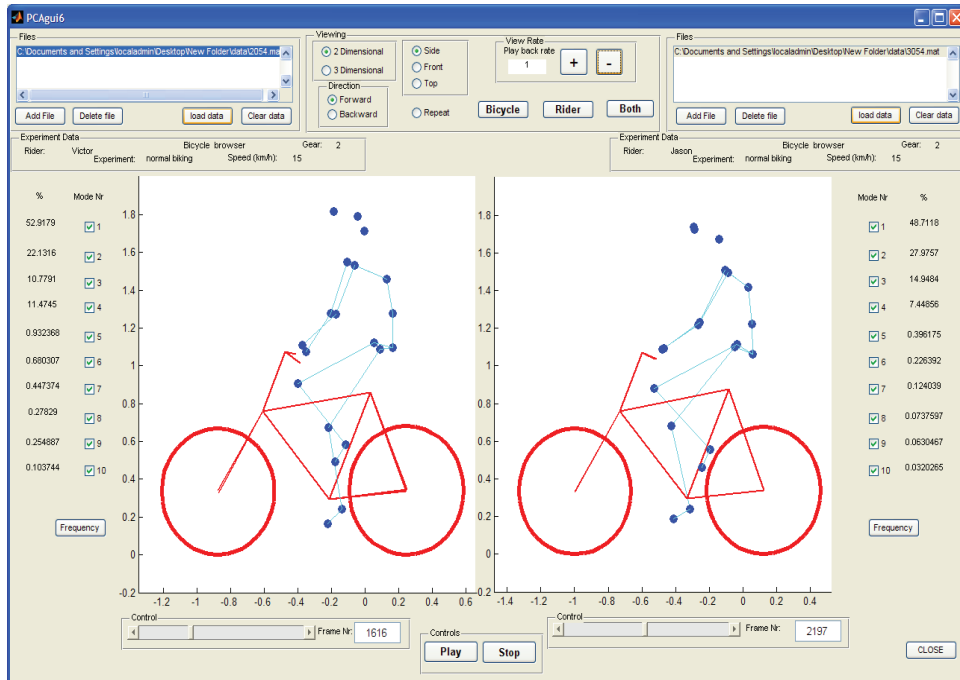


Figure 6: Screen shot of the MATLAB graphical user interface (GUI) used to visualize principal components and compare between different components and trials.

#### 4.4 Data Visualization

We developed a graphical user interface in MATLAB that easily allows different trials to be compared with one another Fig. (6). The program loads in two different trials along with information on the trial. A graphical representation of the rider and bicycle are displayed in two adjacent screens and can be viewed from multiple perspectives. The animations of the runs can be played at different speeds, rewind and fast forwarded. The principal components are shown beside the corresponding animation display and combinations can be turned on and off for identification and comparison. Frequency and amplitude information for the temporal coefficients  $a_{ij}$  can also be displayed for comparison.

### 5 RESULTS

#### 5.1 Motion identification

The reduced set of data provides two important pieces of information for the identification of motion: the principal components  $v_i$  and the corresponding coefficients  $a_{ij}$ . The principal components represent linear trajectories of the markers and the coefficients show how the markers follow the trajectories with time. We began processing the data by reviewing each principal component of each trial in the GUI and noting down what type of motion we saw Tab. (1). These descriptions were subjective because we grouped marker movement based on our preconceived understanding of rider and bicycle motion. Some of the modes displayed motions that were not physically possible such as the upper leg stretching in length during the knee bounce. This is possible when examining a single component but when superimposed over the rest of the components the unrealistic motions are not present. Furthermore, for each component we examined amplitude and frequency content of the associated coefficients  $a_{ij}$  as shown in Fig. (7) and noted down the shape of the frequency spectrum and the frequencies at any distinct spikes.

$i$	% Variance	Motion Description	Frequency Description
1	45.50	primarily longitudinal motion, some lateral	max amp=0.6m, most freq below 0.5hz, tiny spike at 1.6hz
2	29.39	primarily lateral motion, some longitudinal, small feet motion	little spike at 0.8hz, max amp=0.35m, most freq below 0.5hz
3	15.41	vertical pedaling, slight spine bend, hip/head/shoulder sway out of phase with pedaling	large dominant spike at 0.8hz, max amp=0.27m
4	8.27	horizontal pedaling, head/shoulder sway	large dominant spike at 0.8hz with 0.19m amp
5	0.82	yaw, knees stay still	most freq below 1hz, spike at 0.33hz and 0.04m
6	0.27	erratic left hand movement	max amp=0.018hz, most freq. below 2hz
7	0.21	steer, left hand movement, slight roll	most freq below 2hz, spike at 0.33hz and 1.58hz
8	0.07	knee and head bounce	dominant spike at 1.58hz
9	0.04	lat knee movement, head jiggle	spikes at 1.58hz and 2.37hz, most freq below 2.5hz
10	0.02	head and knee jiggle	spikes at 1.58hz and 3.17hz, most freq below 3.5hz

Table 1: Example raw trial description for the bicycle and rider during normal pedaling at 10 km/h.

Several conclusions can be drawn from examining the coefficient data. First of all, some of the components are linked by the frequencies of the coefficients and describe an identifiable motion. The most obvious being that the vertical and horizontal pedaling components make up the circular pedaling motion. They both vary periodically and have a dominant frequency which is defined by the cadence. In the example trial, Tab. (1), the upper body motions are also linked to the pedaling. Components 8 and 9 are both based around a frequency that is twice the pedaling frequency which may be due to the forces created at each pedal stroke. Component 6 seems to be the result of a bad marker signal. Components 5 and 7 are interesting because they display motions of the bicycle that are not dominated by the pedaling frequency and may be candidate control motions. The percentage variance of each component gives an idea of the relative amplitude of the components. The descriptions of each trial were used to compile a list of motions that contribute to the principal components. These motions, illustrated in Fig. (8), are:

**Drift** The bicycle and rider drift longitudinally and laterally on the surface of the treadmill. The motions are typically defined by two components that are not necessarily orthogonal or aligned with the inertial coordinate system. The motion is random and at low frequencies.

**Steer** Rotation of the front assembly with respect to the rear frame. The steering may appear linked to one of the pedaling components at the pedaling frequency or may be in one or more components sometimes combined with roll and/or yaw at more random frequencies, Fig. (8a).

**Roll** The bicycle and the rider roll with respect to the ground plane. Roll is typically linked with steer and/or yaw and often at the pedaling frequency, Fig. (8a).

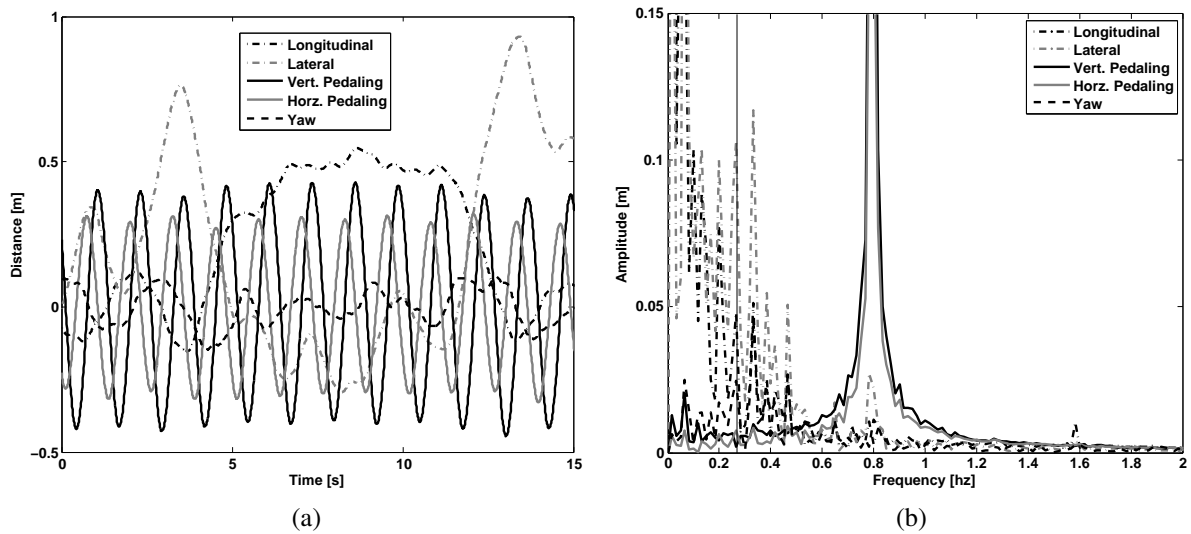


Figure 7: (a) Coefficients  $a_{ij}$  versus time and (b) the frequency content of the first five principal components for normal pedaling at 10 km/h. The vertical line in (b) represents the open loop weave frequency (0.28hz) determined from Fig. (4) at this forward speed .

**Yaw** The heading angle of the bicycle and rider change together with respect to the ground plane. This is typically linked with steer, roll and/or the drift, Fig. (8b).

**Pedaling** This motion is defined by two or more components, typically a vertical and horizontal motion of the feet, that show the feet rotating around the crank axle at a distinct frequency and the legs following suit, Fig. (8c).

**Bend** The spine bent laterally and was always connected with the vertical pedaling component, Fig. (8d).

**Lean** The upper body, shoulders and head lean laterally with respect to the rear frame and was always linked with the horizontal pedaling component, Fig. (8e).

**Twist** The shoulders rotate about the torso axis. This was linked to components that contained steering motions both random and at the pedaling frequency, Fig. (8f).

**Bounce** The knee markers bounce up and down, the back straightens and the head nods at twice the pedaling frequency, Fig. (8g).

**Knees** The knees move laterally relative to the bicycle frame in both opposing directions and the same direction at random low frequencies, Fig. (8h).

**Head** Head twists and random head motions showed up often. These seemed to be due to the rider looking around randomly.

## 5.2 Motion Identification and Characterization

To identify how bicycling changes with speed it would be ideal to investigate how the amplitude of each component varies with speed. However as the analysis does not return the

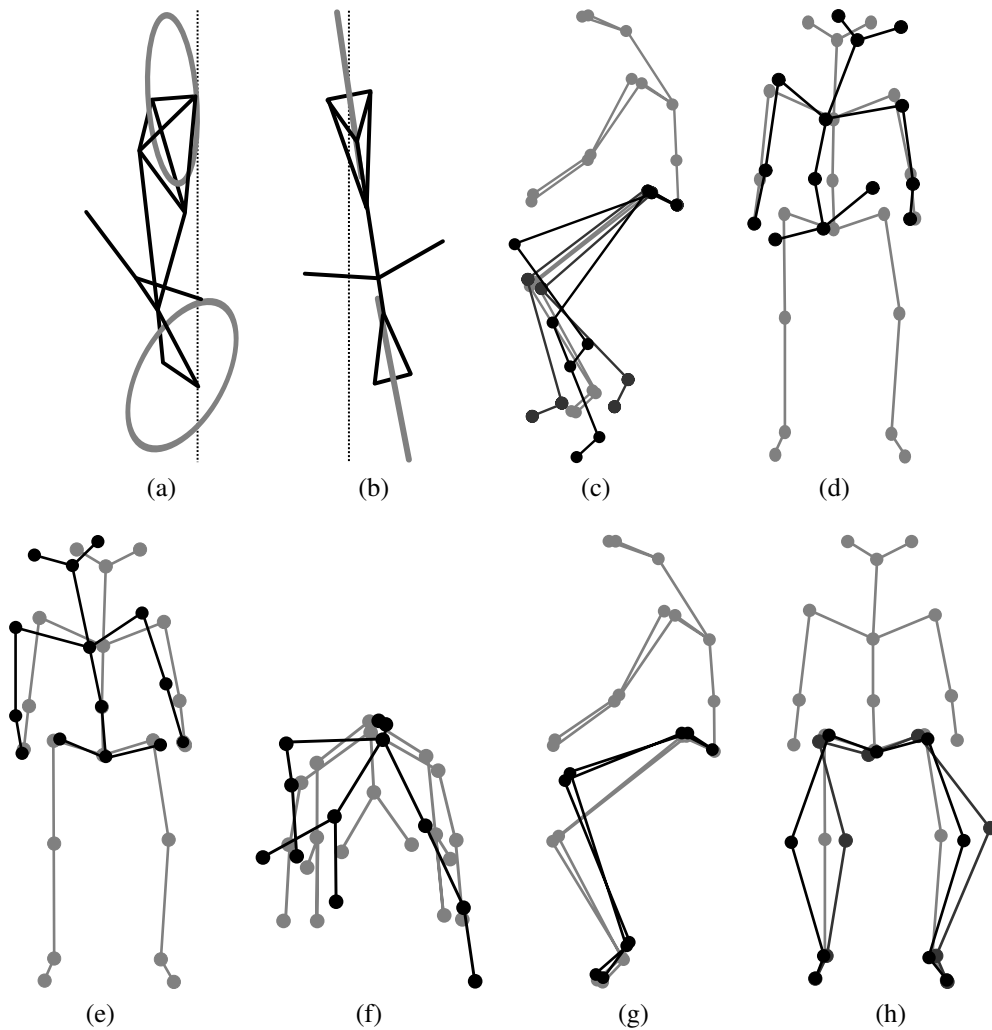


Figure 8: Diagrams of the common motions. (a) Top view of the bicycle steer and roll, (b) the bicycle yaw, (c) the horizontal and vertical components of pedaling, (d) the spine bend, (e) rider lean, (f) top view of the rider twist, (g) knee bounce and (h) two knee motions. All but the pedaling are exaggerated for clarity.

same set of components for each run such a comparison is typically not possible. Therefore components were grouped into classes, where each class shows a specific physically relevant motion. The same total motion of the class can be described by one set of components in one trial and another, probably different, set of components in another trial. How the amplitudes of these classes change between two experiments can be used as a measure for how bicycling has changed among trials.

To objectively identify which coefficients show the same type of motion and could therefore form a class, the frequency content of each of the time coefficients in a single trial was correlated to that of each of the other components in that trial. Next a minimum correlation value was set to determine which coefficients were correlated to each other. When the minimum was set at 0.9 only the coefficients making up the pedaling motion could be considered correlated. On the other hand when a minimum level of 0.7 was used practically every coefficient was correlated to each other. The only exception was the coefficient that displayed the bounce.

Its maximum correlation with another coefficient was no higher than 0.4 for any of the tested speeds. The 0.8 level gave a number of distinct classes of components and thus this level was used to identify which coefficients were connected. Finally, the correlated coefficients were viewed simultaneously in the GUI enabling the determination of the motion class.

The correlated coefficients were used to form six different classes of motions, each made up of combinations of the previously described motions, with reference to Fig. (8):

**Drift** Drift.

**Pedaling** Pedaling (8c), Bend (8d), Lean (8e), Twist (8f).

**Steer-Yaw-Roll** Steer and Roll (8a), Yaw (8b).

**Bounce** Bounce (8g).

**Knees** Knees (8h).

**Others** Head and components that showed noise of some sort.

In most cases the correlated coefficients described a single class. However, in some cases this was not the case and the coefficients were used to describe more than one class. An example is that at low speed the components containing the drift motions also contained large steer, yaw and roll motions. Therefore, the motions were placed in both the Drift and the Steer-Yaw-Roll classes.

Since the rider was not instructed to hold a specific location on the treadmill the Drift class, which was usually the class with the largest amplitude, was not used in further analysis of the motion and neither was the 'Other' class. For each of the remaining classes, the percentages of variance of the remaining components were recalculated without the components placed in the Drift and the Other classes.

By transforming the bicycle marker locations into rigid body motions for the bicycle (See Appendix A) it was also possible to investigate the bicycle lean, yaw and steering motions. By carrying out a Fourier transform these bicycle motions could also be investigated in the frequency domain.

### 5.3 Characterization of motions during normal pedaling

Figure (9) shows how the percentage of the four classes: Pedaling, Steer-Yaw-Roll, Bounce and Knees vary with speed. From the graph it is clear that at 10 km/h and higher speeds practically all the motion that is taking place is the pedaling motion class. Below 10 km/h, the Steer-Yaw-Roll class becomes increasingly active and the relative percentage of the motion taking place in the pedaling class drops. Also at speeds below 10 km/h the lateral knee motion (Knees) class percentage increases with decreasing speed. The increase is not as significant as that of the Steer-Yaw-Roll class (increase to roughly 5% at 2 km/h), but it is certainly visible. The Bounce roughly remains constant at all speeds.

The steer angle amplitude-frequency plot for each of the speeds calculated from the bicycle rigid body motions is given in Fig. (10). It clearly shows that the steering actions take place at (high speed) or around (low speed) the pedaling frequency. It also shows that the amplitude of the steering angle increases by 5000% when the speed decreases from 30 km/h to 2 km/h. Figure (10) also shows the open loop, rigid rider, weave eigenfrequency for each speed obtained from Fig. (4). Apparently the open loop eigenfrequency is not a frequency in which the bicycle/rider operates.

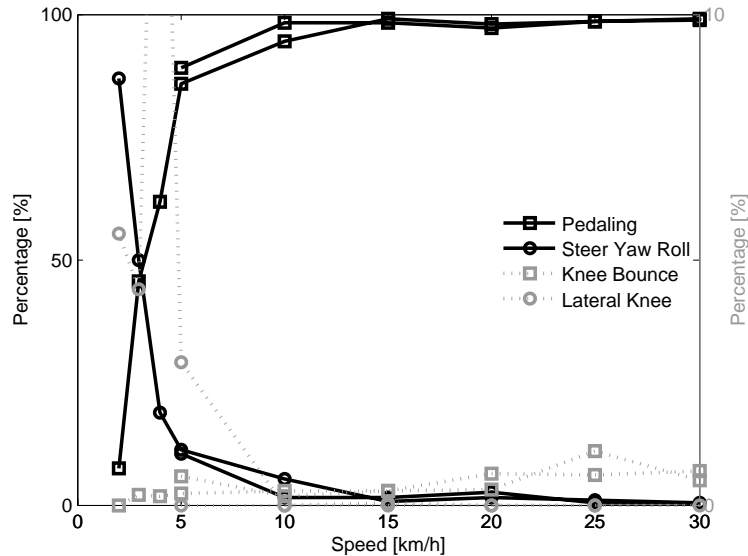


Figure 9: The percentage of the motion from each of the four classes: Pedaling, Steer-Yaw-Roll, Bounce and Knees, at the different speeds when the Drift and ‘Other’ classes were removed from the results for normal pedaling. The solid lines are scaled to 100% (left axis), the dotted lines are scaled to 10% (right axis).

#### 5.4 Characterization of motions without pedaling

At normal pedaling, all motions, including the control tasks, are dominated by the pedaling motions. Therefore we also looked at the motions bicycle/rider system without the influence of pedaling. Figure (11) shows how the percentage of the motion caused by Steer-Yaw-Roll, Bounce and Knees varies with speed. Since the bicycle is towed and the riders feet remain in the same, constant, position relative to bicycle, there is no pedaling class present in analysis. Furthermore, no bend, lean or twist motions were detected during the experiments.

It is clear that at all speeds most motion takes place in the Steer-Yaw-Roll class. Also interesting is that unlike in the normal pedaling situation, the Knee motion percentage does not increase at low speeds.

Figure (12) shows the bicycle rigid body steer angle frequency-amplitude plot for different speeds. Compared to the normal pedaling the amplitudes are about half the size at the low speeds and one tenth the size at high speeds, indicating that smaller steering angles were made. The frequency content now also shows a much wider, flatter spectrum compared to normal pedaling. At 10 and 15 km/h the frequency with the largest amplitude is near the open loop weave eigenfrequency. However, at the other speeds this is not the case, once again indicating that the rigid body open loop weave eigenfrequency is not the frequency in which the bicycle is controlled.

## 6 CONCLUSIONS

From the analysis on the measured rider motions during normal bicycling by means of principal component analysis we come to the following conclusions:

- During normal bicycling the dominant upper body motions: lean, bend, twist and bounce, are all linked to the pedaling motion.
- We hypothesize that lateral control is mainly done by steering since we observed only

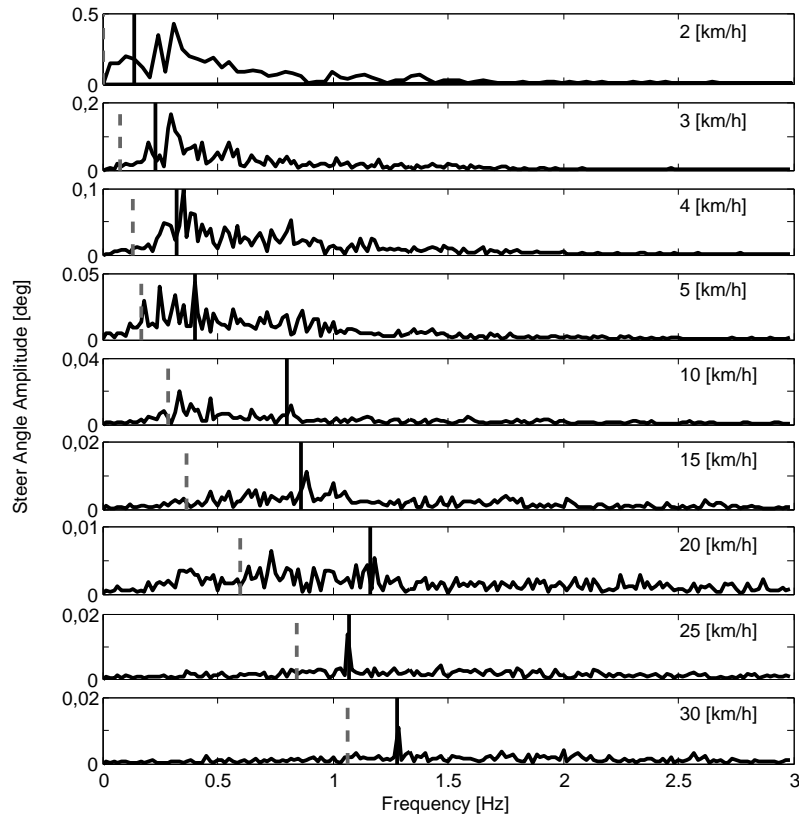


Figure 10: Steer angle amplitude plot for the nine different speeds for normal pedaling experiment. Solid vertical line indicates the pedaling frequency. Dashed vertical gray line indicates the bicycle & rigid rider open loop weave eigenfrequency from Fig. (4).

upper body motion in the pedaling frequency.

- If upper body motions are used for control then this control is in the pedaling frequency.
- When pedaling at low speed we observe lateral knee motions which are probably also used for control.

Future work will be directed in answering the remaining questions listed in Sec. (2).

## 7 ACKNOWLEDGEMENTS

We would like to thank Knoek van Soest and Richard Casius of the Faculty of Human Movement Sciences at the Vrije Universiteit for their cooperation and use of their equipment for the experiments and for Richard's expertise and help in operating the motion capture system and data processing. We would also like to thank the Dutch bicycle manufacturer, Batavus, for supplying the bicycles.

## REFERENCES

- [1] I. T. Jolliffe. *Principal Component Analysis*. Springer Series in Statistics. Springer-Verlag, 1986.
- [2] J. D. G. Kooijman and A. L. Schwab. Some observations on human control of a bicycle. In I. Zobory, editor, *11th mini Conference on Vehicle System Dynamics, Identification and*

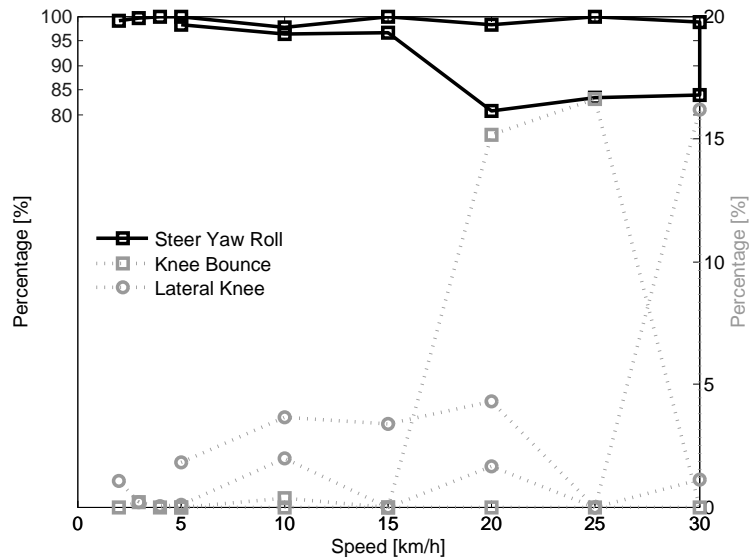


Figure 11: The percentage of the motion from each of the three classes: Steer-Yaw-Roll, Bounce and Knees, at the different speeds when the Drift and ‘Other’ classes were removed from the results for trials without pedaling. The solid lines are scaled to 100% (left axis), the dotted lines are scaled to 20% (right axis).

*Anomalies (VSDIA2008)*, Budapest, Hungary, page 8. Budapest University of Technology and Economics, Nov. 2008.

- [3] J. D. G. Kooijman, A. L. Schwab, and J. P. Meijaard. Experimental validation of a model of an uncontrolled bicycle. *Multibody System Dynamics*, 19:115–132, 2008.
- [4] J. P. Meijaard, Jim M. Papadopoulos, Andy Ruina, and A. L. Schwab. Linearized dynamics equations for the balance and steer of a bicycle: A benchmark and review. *Royal Society of London Proceedings Series A*, 463:1955–1982, August 2007.
- [5] Jason Moore and Mont Hubbard. Parametric study of bicycle stability. In Margaret Estivalet and Pierre Brisson, editors, *The Engineering of Sport 7*, volume 2. International Sports Engineering Association, Springer Paris, 2008.
- [6] Northern Digital Incorporated. Optotrak Certus Motion Capture System. <http://www.ndigital.com>.
- [7] Dale L. Peterson and Mont Hubbard. Yaw rate and velocity tracking control of a hands-free bicycle. In *International Mechanical Engineering Congress and Exposition*. ASME, 2008.
- [8] A. L. Schwab, J. D. G. Kooijman, and J. P. Meijaard. Some recent developments in bicycle dynamics and control. In A. K. Belyaev and D. A. Indeitsev, editors, *Fourth European Conference on Structural Control (4ECSC)*, pages 695–702. Institute of Problems in Mechanical Engineering, Russian Academy of Sciences, 2008.
- [9] R. S. Sharp. On the stability and control of the bicycle. *Applied Mechanics Reviews*, 61(6):24, November 2008.

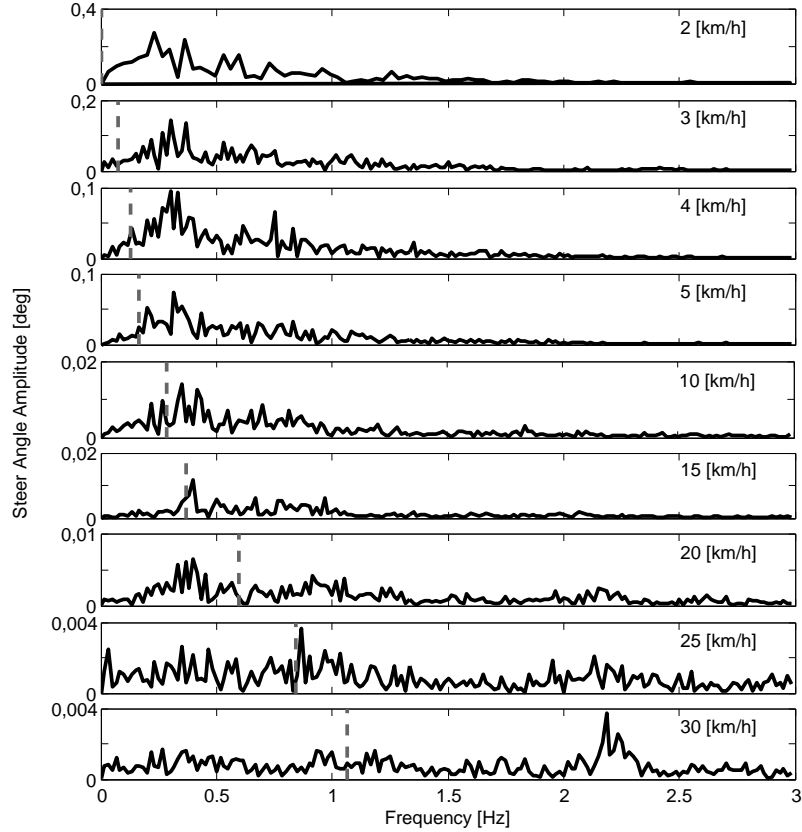


Figure 12: Steer angle amplitude plot for the nine different speeds for the tasks without pedaling. Dashed vertical grey line indicates the bicycle & rigid rider open loop weave eigenfrequency obtained from Fig. (4).

- [10] N. F. Troje. Decomposing biological motion: A framework for analysis and synthesis of human gait patterns. *Journal of Vision*, 2(5):371–387, September 2002.

### A Inertial frames and configuration variables

The transformation from marker coordinates to rigid body inertial frames and configuration variables shown in Fig. (5) is described here. A reference frame,  $\mathbf{N}$ , with origin  $n_o$  corresponding with the benchmark bicycle [4] is defined with respect to the Optotrak reference frame,  $\mathbf{M}$ , Eq. (9).

$$\mathbf{N} = \begin{bmatrix} \hat{\mathbf{n}}_1 \\ \hat{\mathbf{n}}_2 \\ \hat{\mathbf{n}}_3 \end{bmatrix} = \begin{bmatrix} 1 & 0 & 0 \\ 0 & -1 & 0 \\ 0 & 0 & -1 \end{bmatrix} \begin{bmatrix} \hat{\mathbf{m}}_1 \\ \hat{\mathbf{m}}_2 \\ \hat{\mathbf{m}}_3 \end{bmatrix} \quad (9)$$

Thirty-one marker locations were recorded and the vector to each is defined as  $\mathbf{r}^{m_k/n_o}$  where  $k = 1, 2, \dots, l$  for the original markers and  $k = l + 1, \dots$  for any additional virtual markers. To calculate the reference frame attached to the rear bicycle we formed a frame center plane from the seat post marker,  $m_{26}$ , and two new additional virtual markers at the center of the rear wheel,  $m_{36}$ , and the center of the head tube,  $m_{33}$ . For example, the center of the rear wheel was calculated by Eq. (10) where  $m_{25}$  and  $m_{31}$  are the left and right rear wheel markers.

$$\mathbf{r}^{m_{36}/n_o} = (\mathbf{r}^{m_{25}/n_o} + \mathbf{r}^{m_{31}/n_o})/2 \quad (10)$$

The normal vector to the plane through the rear wheel center, seat post and the head tube center is

$$\hat{\mathbf{b}}_2 = \frac{\mathbf{r}^{m_{36}/26} \times \mathbf{r}^{m_{33}/26}}{|\mathbf{r}^{m_{36}/26} \times \mathbf{r}^{m_{33}/26}|} \quad (11)$$

The heading vector of the rear frame is then  $\hat{\mathbf{b}}_1 = \hat{\mathbf{b}}_2 \times \hat{\mathbf{n}}_3$  and  $\hat{\mathbf{b}}_3 = \hat{\mathbf{b}}_1 \times \hat{\mathbf{b}}_2$  follows. These unit vectors define a reference frame that leans and yaws with the rear frame. We assumed that the rear frame pitch is negligible. The marker locations of the rider can now be expressed in the B frame with reference to a point on the rear frame  $m_{36}$ , Eq. (12), and these were used in the PCA of the rider only markers.

$$\mathbf{r}^{m_k/m_{36}} = (\mathbf{r}^{m_k/m_{36}} \cdot \hat{\mathbf{b}}_1)\hat{\mathbf{b}}_1 + (\mathbf{r}^{m_k/m_{36}} \cdot \hat{\mathbf{b}}_2)\hat{\mathbf{b}}_2 + (\mathbf{r}^{m_k/m_{36}} \cdot \hat{\mathbf{b}}_3)\hat{\mathbf{b}}_3 \quad (12)$$

A reference frame  $\mathbf{D}$  that is aligned with the steering axis of the rear frame can be formulated by rotation about the  $\hat{\mathbf{b}}_2$  axis through the steer axis angle  $\lambda$  which is measured from each bicycle.

$$\mathbf{D} = \begin{bmatrix} \hat{\mathbf{d}}_1 \\ \hat{\mathbf{d}}_2 \\ \hat{\mathbf{d}}_3 \end{bmatrix} = \begin{bmatrix} \cos \lambda & 0 & -\sin \lambda \\ 0 & 1 & 0 \\ \sin \lambda & 0 & \cos \lambda \end{bmatrix} \begin{bmatrix} \hat{\mathbf{b}}_1 \\ \hat{\mathbf{b}}_2 \\ \hat{\mathbf{b}}_3 \end{bmatrix} \quad (13)$$

The handlebar/fork inertial frame  $\mathbf{E}$  is then calculated by defining the  $\hat{\mathbf{e}}_2$  to be aligned with front wheel axle Eq. (14).

$$\hat{\mathbf{e}}_2 = \frac{\mathbf{r}^{m_{21}/n_o} - \mathbf{r}^{m_{27}/n_o}}{|\mathbf{r}^{m_{21}/n_o} - \mathbf{r}^{m_{27}/n_o}|} \quad (14)$$

The handlebar/fork frame rotates around  $\hat{\mathbf{d}}_3 = \hat{\mathbf{e}}_3$  and then  $\hat{\mathbf{e}}_1 = \hat{\mathbf{e}}_3 \times \hat{\mathbf{e}}_2$ . The instantaneous rear wheel radius is

$$r_{\mathbf{R}} = -\frac{\mathbf{r}^{m_{36}/n_o} \cdot \hat{\mathbf{n}}_3}{\hat{\mathbf{b}}_3 \cdot \hat{\mathbf{n}}_3}. \quad (15)$$

This is used to formulate the vector to the rear wheel contact point Eq. (16).

$$\mathbf{r}^{m_{39}/n_o} = \mathbf{r}^{m_{36}/n_o} + r_{\mathbf{R}}\hat{\mathbf{b}}_3 \quad (16)$$

This now allows us to calculate six of the eight configuration variables of the bicycle as a function of time.

$$\text{Distance to the ground contact point: } q_1 = \mathbf{r}^{m_{39}/n_o} \cdot \hat{\mathbf{n}}_1 \quad (17)$$

$$\text{Distance to the ground contact point: } q_2 = \mathbf{r}^{m_{39}/n_o} \cdot \hat{\mathbf{n}}_2 \quad (18)$$

$$\text{Yaw angle: } q_3 = \arccos(\hat{\mathbf{b}}_1 \cdot \hat{\mathbf{n}}_1) \quad (19)$$

$$\text{Roll angle: } q_4 = \arccos(\hat{\mathbf{b}}_3 \cdot \hat{\mathbf{n}}_3) \quad (20)$$

$$\text{Pitch angle: } q_6 = 0 \quad (21)$$

$$\text{Steer angle: } q_7 = \arccos(\hat{\mathbf{d}}_1 \cdot \hat{\mathbf{e}}_1) \quad (22)$$